Solute Transport through the Austin Chalk Weathered Zone at the SSC Site

Final Report

by

Robert E. Mace

Alan R. Dutton
Principal Investigator

Prepared for

Texas National Research Laboratory Commission
under Contract No. IAC 94-0108

Bureau of Economic Geology
Noel Tyler, Director
The University of Texas at Austin
Austin, Texas 78713-8924

August 1995

CONTENTS

Figures

Tables

INTRODUCTION

The purpose of this work is to better understand the occurrence and movement of ground water and the transport of solutes in near-surface Austin Chalk in the vicinity of the Superconducting Super Collider (SSC) site. The scope of work includes (1) further characterization of the hydrogeological attributes of the weathered zone pertinent to solute transport and (2) numerical simulation of ground-water flow and solute transport to estimate solute transport time and paths. This work determines transport times and relative solute concentrations in the vicinity of spoil piles, the linear accelerator, or other potential sources of contamination at the SSC site. The results summarized in this report will be useful for assessing the risk of solute migration from the SSC site and evaluating short- and long-term monitoring needs.

This report presents the results of (1) further characterization of the weathered zone, (2) interpretive models generalized for average weathered-zone properties and environment, and (3) three-dimensional modeling of ground-water flow and solute transport at the West Campus of the SSC. Characterization and modeling work focuses on the hydrologic and geographic setting of the West Campus, which can be used as an analog for flow and transport beneath spoil piles located at the access sites at various locations on the SSC footprint underlain by Austin Chalk.

This study builds on hydrogeologic work previously accomplished in the Austin Chalk. Previous work includes preliminary hydrologic work in deep chalk (Earth Technology Corporation, 1990), an assessment of the occurrence and movement of ground water in deep and shallow Austin Chalk (Dutton and others, 1994), records of water levels in deep and shallow wells (Mace and Dutton, 1994a), and hydrologic studies in fractured chalk (Mace, 1994). Mace and Dutton (1994b) used the information presented in these reports to hypothesize that fracture intensity, rainfall, water-table elevation, and fracture coatings are important controls on contaminant transport in weathered and fractured chalk. This report addresses these issues and quantifies their effects using analytical and numerical models.

METHODS

The approach for this study was to (1) characterize the important hydrogeologic controls on flow and transport through the weathered zone and (2) use several different models to understand and quantify flow and transport in weathered Austin Chalk. This approach involved additional field mapping, statistically describing hydrogeologic properties, and using the developed conceptual model and statistical descriptions to generate realistic numerical models.

Hydrogeologic Characterization

Before modeling, the hydrologic and geometric properties of the weathered zone were characterized and mathematically described. These mathematical descriptions were used to create generalized flow and transport models as well as stochastic models of more specific sites. Variability of hydraulic conductivity and porosity with depth, thickness of the weathered zone, and topography and its relationship to ground-water gradients were the physical properties that were further characterized during this study. In addition, coefficients applicable to the fractured chalk at the SSC site were estimated based on a literature search.

Variation of Hydraulic Conductivity and Porosity with Depth

The variation of hydraulic conductivity and porosity with depth is very important in assessing flow and transport through the weathered zone. Dutton and others (1994) established the spatial variability of transmissivity in the weathered zone and noticed that aquifer tests performed at different initial water levels in the same well resulted in different transmissivities. These tests showed that weathered zone transmissivities were smaller with increasing depth to water and that the difference could not be solely explained by smaller saturated thicknesses.

The aquifer tests were further analyzed to determine the hydraulic conductivity for the specific tested intervals by using an algebraically altered harmonic mean:

$$K_b = \frac{\overline{K}b - K_a b_a}{b_b} \tag{1}$$

where K_b is the hydraulic conductivity of interval b, $\overline{K}$ is the hydraulic conductivity of the entire interval, b is the length of the entire interval, K_a is the hydraulic conductivity of interval a, b_a is the length of interval a, and b_b is the length of interval b. In this manner, the distribution of hydraulic conductivity with depth could be ascertained.

Because hydraulic conductivity appeared to decrease exponentially with depth in the weathered zone, a negative exponential was fit to the data:

$$K = A\exp^{-Bz} \tag{2}$$

where K is hydraulic conductivity, z is depth below land surface, and A and B are fitting parameters. With this equation, hydraulic conductivity could be estimated for any position with depth for input to numerical models.

Because hydraulic conductivity decreases with depth in the weathered zone and is dependent upon fractures, it follows that the fracture porosity also decreases with depth. However, it is very difficult to measure fracture porosity without the aid of tracer tests, which were not conducted in the weathered zone. Direct measurements were not possible owing to safety concerns of entering the wells as well as problems associated with weathering of the well surface or the influence of well construction on wall fractures. Therefore we derived an equation based on the cubic law to estimate fracture porosity, n_f, at depth:

$$n_f = \frac{e}{L} = \frac{(12k_m L)^{1/3}}{L} \tag{3}$$

where e is fracture aperture, L is the thickness of the interval, and k_m is the intrinsic permeability of the interval at the equivalent porous medium scale (derivation shown in appendix A). In this manner, fracture porosity could be estimated at depth for numerical modeling.

Thickness of the Weathered Zone

Most of the ground water traveling through the Austin Chalk moves through the weathered zone. Mace (1993) and Dutton and others (1994) found from numerical models that 97 percent of the flow through the chalk was through the weathered zone, with lesser amounts through unfractured chalk and localized fault zones. Therefore, the weathered-zone thickness defines the depth in which most flow and transport will occur in the chalk owing to the surface release of a solute. The weathered zone is identified in outcrop and in core by oxidized chalk that is tan in color and heavily fractured, especially close to land surface. Collins and others (1992) and Dutton and others (1994) determined the weathered-zone thickness based on well core collected at the SSC site. In this report, their data as well as data from numerous new wells drilled at the SSC site were used to determine mean weathered-zone thickness and the relationship between weathered-zone thickness and topographic setting. Furthermore, detailed measurements of weathered-zone thickness along exposures were analyzed to determine spatial variability.

Measurements of Austin Chalk soil and weathered-zone thickness were compiled from contractor reports on boreholes drilled at the SSC site. Each well was classified in three topographic settings— (1) hilltop (high topographic setting), (2) valley (low topographic setting), or (3) intermediate between the hilltop and valley—by inspection of 1:24000 U.S. Geological Survey (USGS) topographic maps. Statistics were used to ascertain relationships between topography and weathered-zone and soil thickness.

Topography and Gradients

Because the weathered zone is limited in depth, topography is very important in defining flow direction and ground-water gradients. Topographic slope is an analog for the magnitude and direction of ground-water gradients affecting solute transport. Therefore, topography of the West Campus area was used to constrain ground-water gradients for the generalized flow and transport

models. This was accomplished by (1) downloading USGS digital elevation models, (2) calculating slopes, and (3) statistically describing the slopes.

A USGS digital elevation model (DEM) of the 1:1,000,000 Dallas sheet, which defined elevation every 310 ft (94 m), was downloaded from USGS computers over the Internet. This file was loaded into ARC/INFO GIS, values for several missing points were interpolated, and elevations for the West Campus area were saved to a file. A FORTRAN program was written using a four-point vector approach to determine the slopes of the topography. The distribution, changes with scale, and spatial relationships of the slopes were quantified using geostatistics.

Dispersion Coefficients in Fractured Rocks

Dispersivity is a physical description of the mixing and spreading that a solute undergoes when transported through porous media. Because dispersivity depends on scale, small-scale measurements cannot be used in models of larger scale processes. In order to definitively determine dispersivity at a large scale, one has to conduct a tracer test at that scale. Oftentimes, this is impractical or infeasible. Gelhar and others (1985) have documented that, in general, different hydrologic systems have similar dispersivities. Therefore, one can use a dispersivity determined at another site as a reasonable approximation for the site at hand. To show that this is also applicable in fractured rocks, dispersivities and the scale at which they were measured were compiled from the literature, and a relationship between dispersivity and scale for fractured rocks was obtained. This relationship was used to determine diffusivity for transport simulations.

Modeling

The modeling approach involved first using simple, general models and then using more complex, site-specific models. This approach was used so that (1) generalizations concerning flow and transport in the weathered zone could be applied to a variety of SSC locations and (2) an understanding of the physical processes at the small scale could be used to assess the accuracy of

simplified large-scale models. For transport on medium to large scales, the modeling approach involved using (1) a general analytical plume model, (2) a general cross-sectional, equivalent porous medium numerical model, (3) a general cross-sectional, discrete fracture model, and (4) a site-specific, three-dimensional, equivalent porous medium model of the West Campus. For numerical modeling, ground-water flow models were constructed, the results of which were used by the solute transport models to calculate transport times.

Analytical Plume Solution

A two-dimensional analytical plume solution was used as a screening tool and as a first approximation of transport in the weathered zone. This analytical solution is discussed in Bear (1972), Hunt (1978), and Wilson and Miller (1978). The analytical solution was coded into FORTRAN and used with data determined from the weathered-zone characterization. The analytical model assumes (1) complete vertical mixing, (2) homogeneity, (3) isotropy, and (4) constant and unidirectional ground-water velocity. The analytical model was used to determine solute breakthroughs under several different conditions. A general plot was created in order to summarize results.

Cross-Sectional Model of Weathered Zone

A cross-sectional model of the weathered zone was used to determine the sensitivity of flow and transport to variations in (1) vertical distribution of hydraulic conductivity, (2) water levels owing to recharge, and (3) hydraulic gradient. The conceptual model was that of a weathered zone of constant thickness on a hillslope of constant slope. The hypothetical, modeled weathered zone was 20 ft (6.1 m) deep and 1,000 ft (304 m) long. Vertically, the model was divided into 10 layers each 2 ft (0.6 m) thick. Horizontally, the model was divided into 100 cells that were 10 ft (3 m) wide. Elevations were assigned assuming a uniformly sloping land surface with a slope of 0.01.

Hydraulic conductivities were assigned according to the vertical distribution observed at hand-dug well 156-1.

The cross-sectional model was oriented along a flow line so the sides of the model could be treated as no-flow boundaries. The uphill, downhill, and bottom sides of the model were also treated as no-flow boundaries. Recharge was uniformly applied to the top of the model, and discharge was from the top of the model using a drain with the elevation set at the top of the uppermost layer. Ground-water flow was modeled with MODFLOW (McDonald and Harbaugh, 1988) using the wet/dry module (McDonald and others, 1991), and particle paths were modeled with MODPATH (Pollock, 1989). It was assumed that all flow takes place in the fractures and that the fracture network could be modeled as if it were equivalent to porous media.

Steady state models were run under different recharge rates, namely 0.001, 0.005, 0.01, and 0.02 ft d^{-1} (0.0003, 0.0015, 0.003, and 0.006 m d^{-1}). Water levels, particle traveltimes, bulk particle velocity, and local particle velocities were determined for each simulation scenario. Bulk particle velocities refer to the average velocity along a flow path. In other words, bulk particle velocity is the total traveltime divided by the total lateral distance traveled. Local particle velocity refers to the velocity of the particle at a given point in space.

Solute transport was modeled with MT3D (Zheng, 1992), a three-dimensional transport model that links directly with output from MODFLOW. The advection solution scheme used was the method of characteristics (MOC) and the modified method of characteristics (MMOC) using a hybrid first-order Euler and fourth-order Runge-Kutta particle tracking algorithm. Because transport modeling requires extensive computer memory and computation time, simulations with the cross-sectional model started with simple boundary conditions (constant heads at either end) and progressed to the model described previously. In this manner, computation time was kept to a minimum, and the influence of vertical mixing, hydraulic gradients, and recharge on concentration breakthroughs was investigated. Four types of models were run:

- a one-dimensional model with constant heads at the uphill and downhill sides,
- a two dimensional model with constant heads at uphill and downhill sides,

- a two-dimensional model with a constant head boundary at the downhill side and recharge on top, and
- the physical model described previously.

Models 1 through 3 used the cross-sectional model described previously as the physical framework and simply used different boundary conditions. Constant heads were assigned according to the elevation of the top of the saturated weathered zone. Simulations were run for three different water-table positions in the weathered zone: in layer 1, in layer 5, and in layer 8. For the one-dimensional models, the top saturated layer (i.e., layers 1, 5, and 8) was used for simulations. For the two-dimensional models, all the layers below the water table (i.e., layers 1–10, layers 5–10, and layers 8–10) were activated. For the two-dimensional model with recharge, recharge rate was adjusted to position water levels at the top of the desired layer. The solute source was placed in the highest active layer in columns 2 through 4. This placement of the source therefore simulates a surface injection of solutes into the weathered-zone aquifer, which would be similar to leachate leaking into the weathered zone from the spoil and muck piles. Dispersivities were assigned and solute concentrations were monitored according to an observation point placed halfway down the hill at 500 ft (150 m).

Model of Ground-Water Flow and Transport for the West Campus

A three-dimensional model was used to determine flow paths and traveltimes in the weathered zone on the West Campus. Weathered-zone physical and hydrogeological characterization data were used in the model. The area consists of two drainage areas in the southern part of the West Campus with a northern boundary defined by a surface-water divide between drainage to Chambers Creek and Waxahachie Creek, the eastern boundary defined by Baker Branch, the western boundary defined by Greathouse Branch, and the southern boundary by Chambers Creek (fig. 1). Boz Creek was contained within the model boundaries. The dimensions of the modeled area are about 8 mi (13 km) in the north-south direction and 3 mi (5 km) in the east-west direction. The bottom of the modeled area was considered to be a no-flow boundary (unfractured Austin

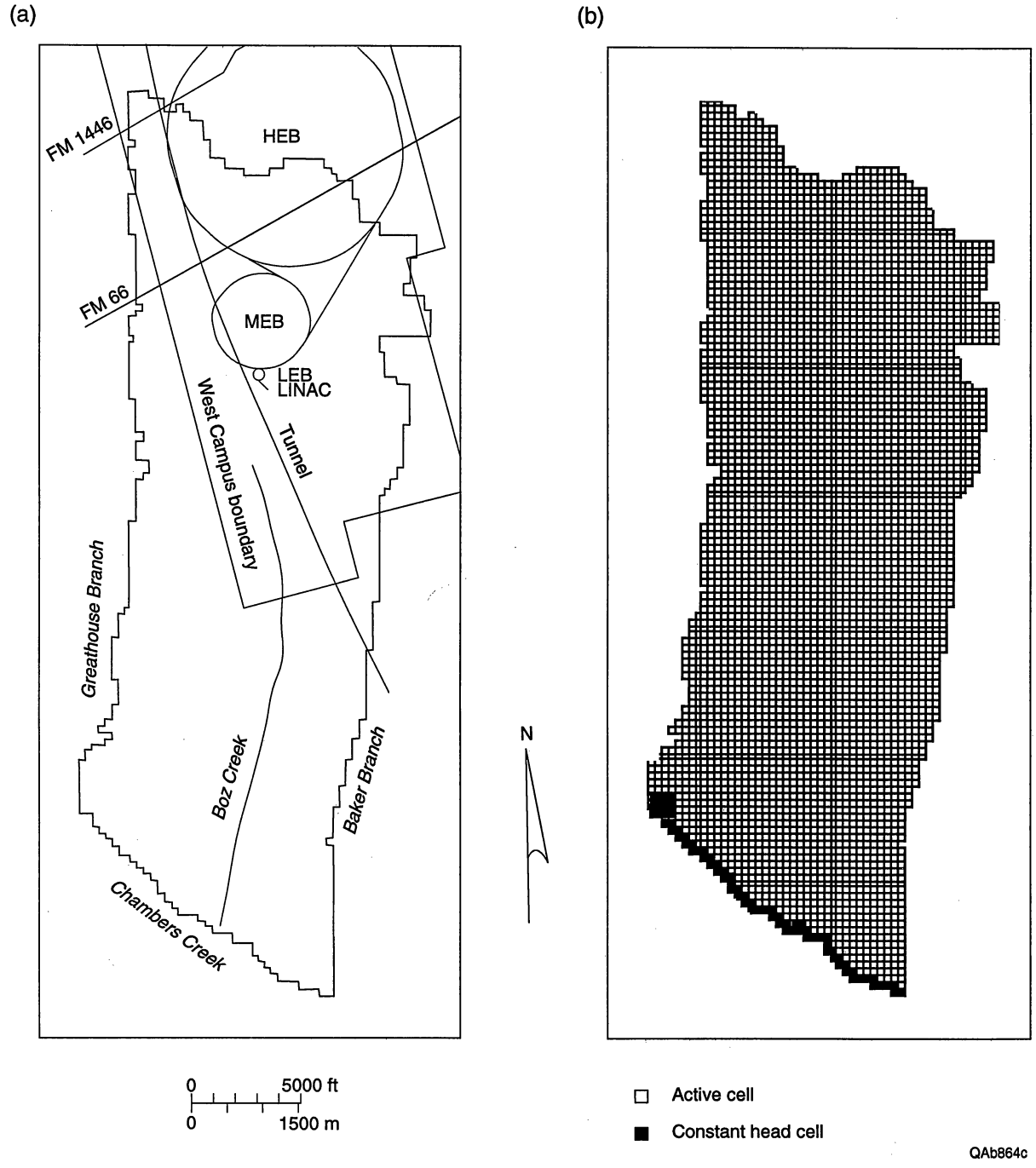

Figure 1. (a) Location of the modeled zone relative to the West Campus. (b) The grid used for modeling. The grid contained 43,700 cells that were 312 by 312 ft in size, 2 ft thick, and arranged in 10 layers.

Chalk), and the top had recharge applied as a constant flux with drains set at land surface at each cell to simulate intermittent springs, seeps, and discharge to local streams. The area was discretized into 53 cells in the east-west direction and 117 cells in the north-south direction, with cell dimensions of 312 by 312 ft (95 by 95 m). The model included 43,700 active cells. Hydraulic conductivity and fracture porosity were assigned the values observed in well 156-1.

Ground-water flow was modeled with MODFLOW (McDonald and Harbaugh, 1988) and particle paths and traveltimes with MODPATH (Pollock, 1989). As in the cross-sectional model, it was assumed that all flow takes place in the fractures and that the fracture network could be modeled as if it were equivalent to porous media.

RESULTS AND DISCUSSION

This section is organized into two parts: a presentation and discussion of results from the characterization studies and a presentation and discussion of results from the modeling studies. At the end of the discussion of the characterization results, a conceptual model of flow and transport in the weathered zone is presented.

Results of Characterization Studies

Variation of Hydraulic Conductivity and Porosity with Depth

In each of the four wells tested, hydraulic conductivity decreases with depth, sometimes over an order of magnitude (fig. 2). Figure 3 shows negative exponential fits to the decreasing permeability with depth. In the case of well 262A-2, the negative exponential provides a suitable fit. The other wells have only two measurements and therefore the exponential is an interpretation of the vertical distribution of hydraulic conductivity in the weathered zone at those sites. Fracture porosity determined using equation 4 is also presented in figure 3 for each of the wells.

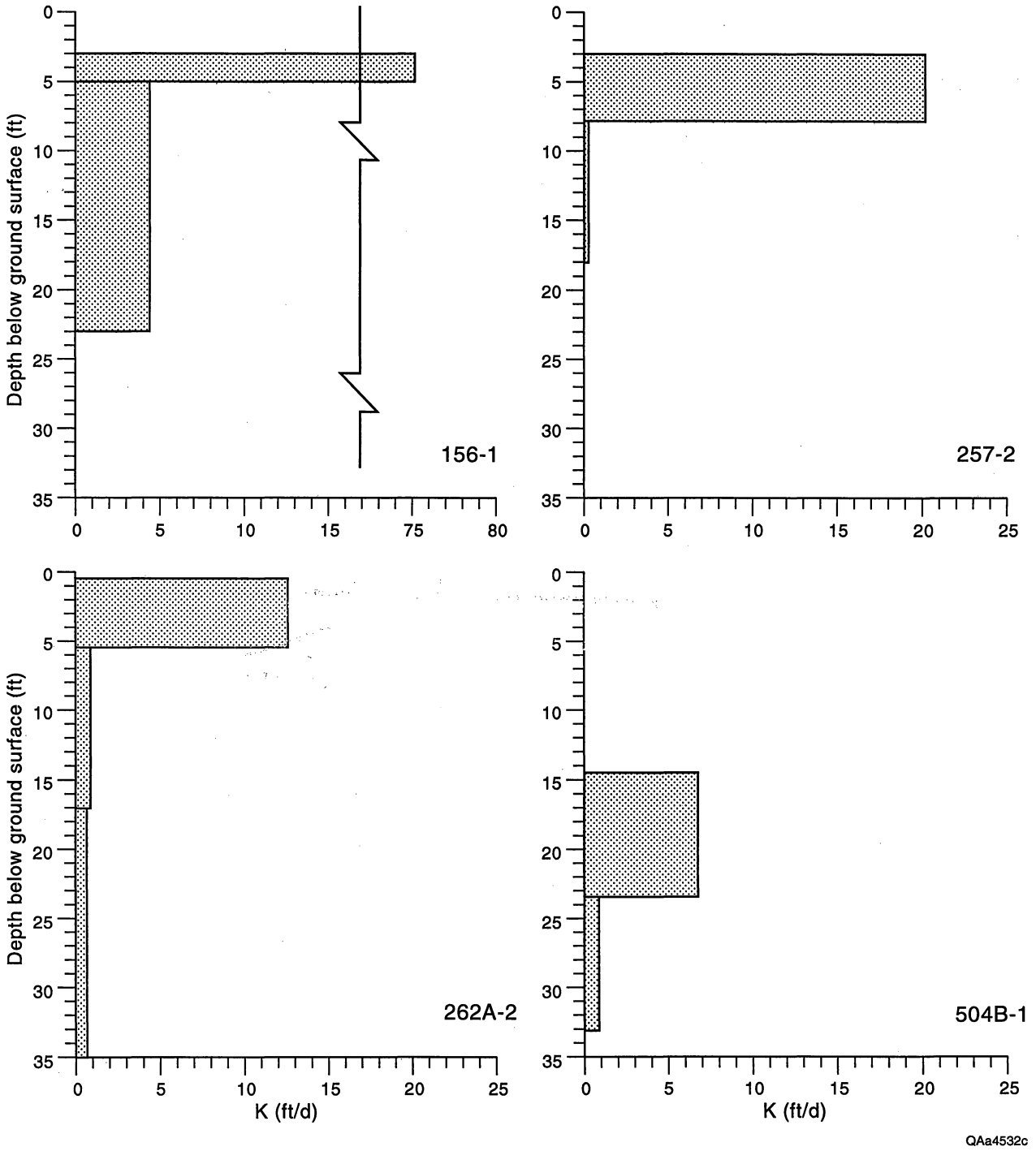

Figure 2. Decrease of hydraulic conductivity with depth in the weathered zone.

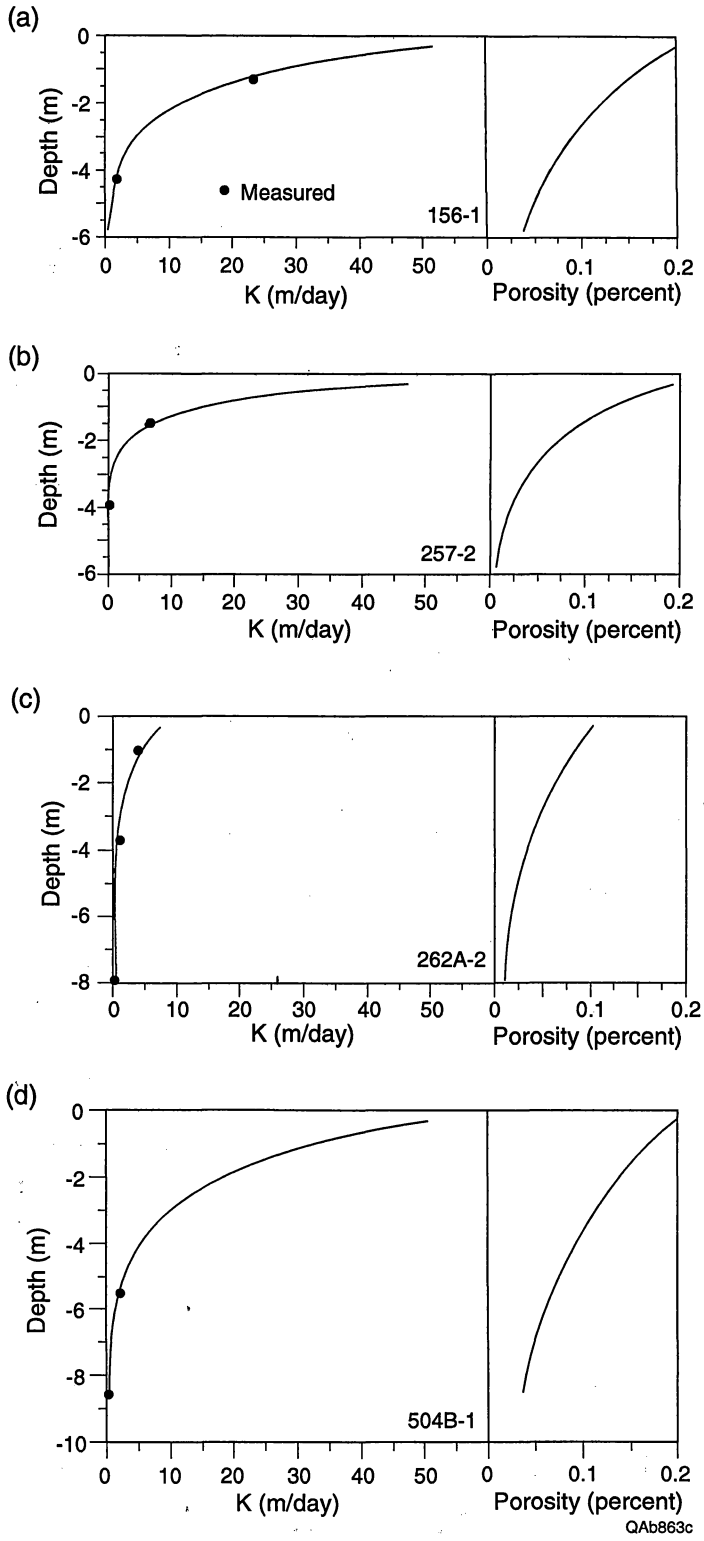

Figure 3. Negative exponential fits to hydraulic conductivity data and corresponding predicted fracture porosity (using eq. 4 in text) at wells (a) 156-1, (b) 257-2, (c) 262A-2, and (d) 504 B-1. Measured values shown at midpoint of tested interval.

Thickness of the Weathered Zone

A list of the wells and the corresponding soil and weathered-zone thickness is provided in appendix B. Histograms of the logarithm of soil and weathered-zone thickness are presented in figure 4a and 4b, respectively. Soil thickness has a nonuniform distribution with a geometric mean of 3.1 ft (0.93 m). Geometric mean ($\bar{x}_g$) of the weathered zone is 8.6 ft (2.6 m). Both soil and weathered-zone thickness distributions can be described with a negative exponential (fig. 4c and 4d, respectively). Two points of weathered-zone thickness have considerably greater weathered thickness and do not fall on the negative exponential. These points have been strongly influenced by large, normal faults that cut through the chalk and therefore are not typical of the chalk in Ellis County.

Table 1 summarizes the statistics of soil and weathered-zone thicknesses for different topographic settings. Weathered-zone thickness does not appear to differ among most topographic settings. However, both soil and weathered-zone thicknesses have considerably different thicknesses in valleys where soils are much thicker and the weathered zone is much thinner.

Table 1. Correlation between soil and weathered-zone thickness to topography.

Topographic setting	Log soil thickness $\bar{x} \pm \sigma$ (m)	Log weathered-zone thickness $\bar{x} \pm \sigma$ (m)
H	-0.14 ± 0.45	0.45 ± 0.24
H, H-M	-0.20 ± 0.45	0.47 ± 0.29
M	0.06 ± 0.51	0.43 ± 0.33
M, M-L	0.03 ± 0.62	0.44 ± 0.32
L, M-L	-0.06 ± 0.59	0.34 ± 0.34
L	0.17 ± 0.62	0.10 ± 0.34
all	-0.03 ± 0.52	0.42 ± 0.32

H = hilltops
M = mid hill
L = hill bottoms

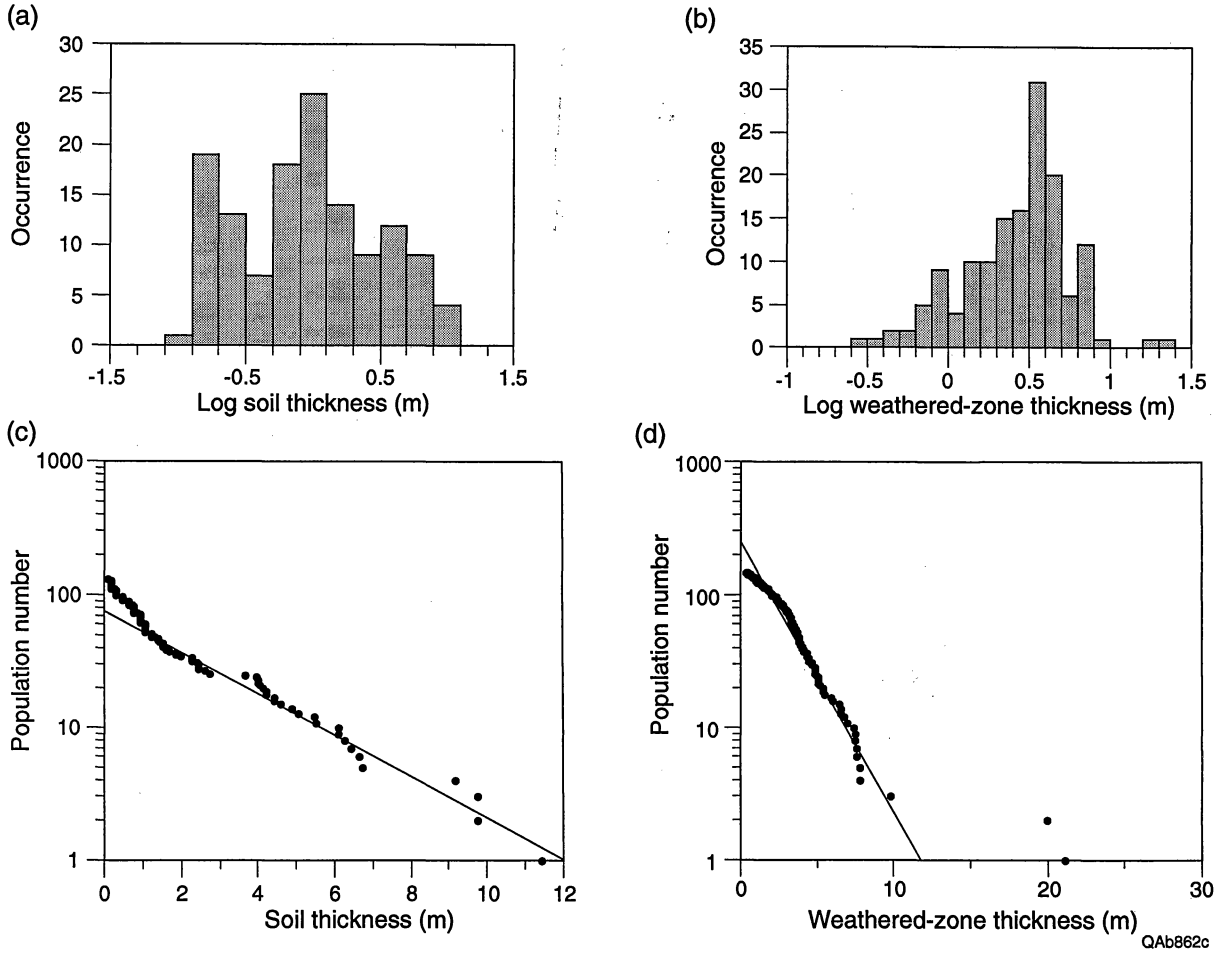

Figure 4. Analysis of soil and weathered-zone thicknesses. Histograms of the (a) log of soil thickness and (b) log of weathered-zone thickness. Negative exponential fit to (c) soil thickness and (d) weathered-zone thickness. The two outliers with weathered-zone thickness greater than 66 ft (20 m) are influenced by regional faulting.

Topography and Gradients

Topography of the West Campus study area was analyzed to estimate ground-water gradients and is shown in figure 5a. Topography regionally slopes toward the southeast, with local slopes to the south and northeast. Figure 5b shows the spatial distribution of slope, which ranges from about 0.01 to 0.1 and indicates that there are alternating zones of low and high slopes. The distribution of slope approximates a log-normal distribution with a geometric mean of 0.018 (fig. 5c). Mean slope is scale dependent: in other words, the slope depends on the distance over which it is measured. Figure 5d shows the influence of scale on slope, with greater mean slopes at smaller scales than larger scales. The semi-variogram shows that slope is spatially correlated within 3,000 to 6,500 ft (1,000–2,000 m) (fig. 5e).

The conclusions from this analysis are that (1) slope is spatially distributed between about 0.01 and 0.1, (2) the mean slope is 0.018, (3) slope is scale dependent, and (4) slope is spatially correlated within 3,000 to 6,500 ft (1,000–2,000 m). A typical slope for 3,000 ft (1,000 m) long hill is 0.01. Because ground-water flow in the weathered zone is strongly controlled by topography, this slope is an analog for the hydraulic gradient and is a representative value for general simulations.

Dispersion Coefficients in Fractured Rocks

Table 2 lists dispersivities in fractured, geologic media measured at different scales. Dispersivity is scale dependent; therefore, the length over which it is measured is important. A log-log plot of dispersivity against scale does not show a strong correlation, though the EPA (1986) estimate for dispersivity in porous media (eq. 4a) lies among most of the measured points (fig. 6). Therefore, the EPA estimate for dispersivity, which is generally used for alluvial deposits, can also be used for fractured rocks. For estimating dispersivity, the EPA suggests using

$$\alpha_L = 0.1 x_r, \text{ and} \qquad (4a)$$

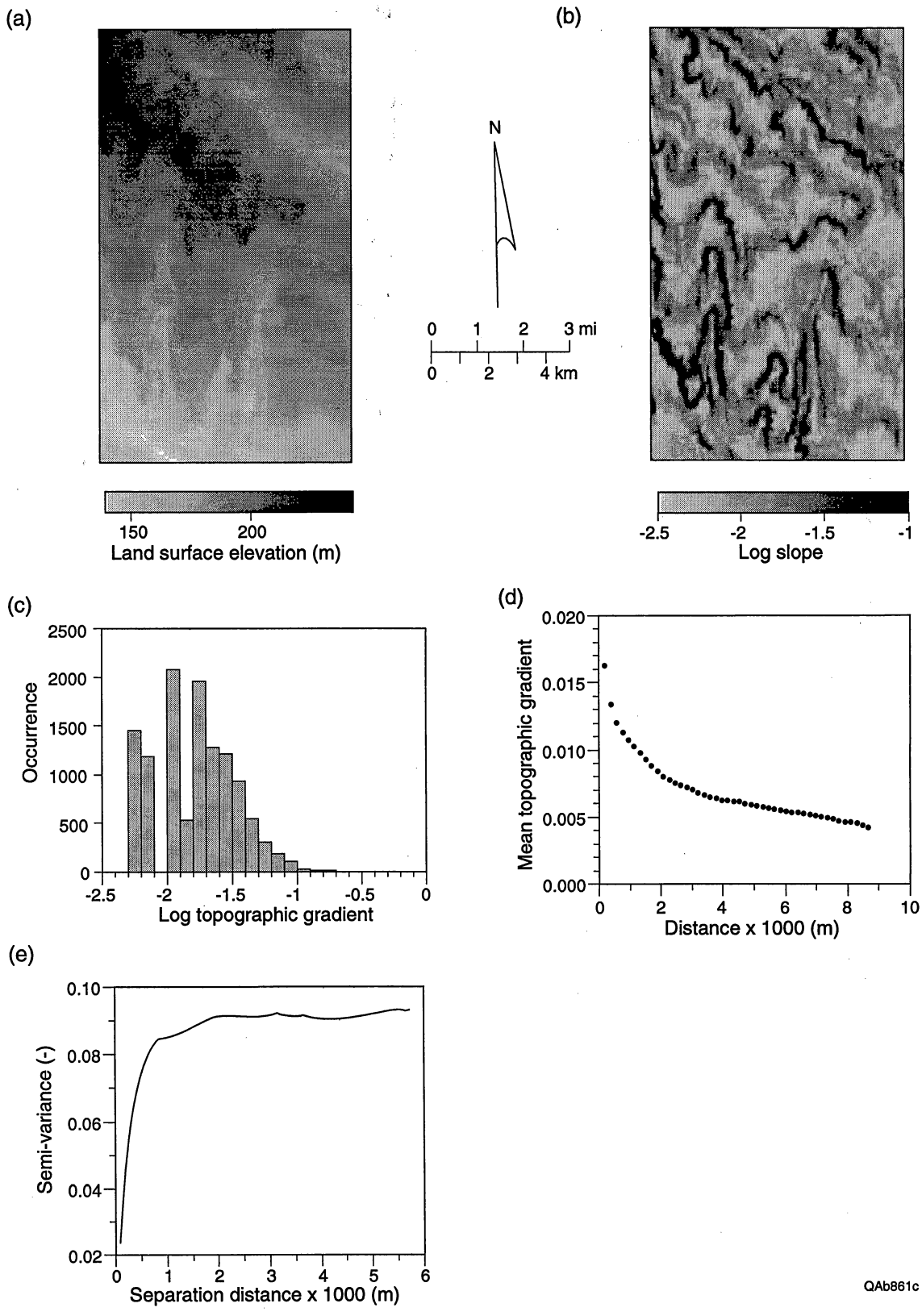

Figure 5. Analysis of topography in the West Campus area. (a) Topography at the site. (b) Spatial distribution of slope. (c) Histogram of slope. (d) Scale effects on the mean slope. (e) Semi-variogram of slope.

$$\alpha_T = \frac{1}{3}\alpha_L. \tag{4b}$$

Vertical dispersivity was determined from

$$\alpha_v = \frac{1}{20}\alpha_L \tag{4c}$$

where α_L is the longitudinal dispersivity, α_T is the transverse dispersivity, α_v is the vertical dispersivity, and x_r is the distance to the receptacle well.

Table 2. Dispersivities measured in different fractured geologic material at different scales.

Reference	Aquifer material (m)	Scale (m)	Dispersivity
Bentley and Walter (1983)	Dolomite	23	5.2
Classen and Cordes (1975)	Dolomite	122	15
Dieulin (1981)	Granite	6	0.5
Goblet (1982)	Granite	17	2
Grove and Beetem (1971)	Dolomite	55	38.1
Haldeman and others (1991)	Tuff	0.5	0.0207-8.01
Ivanovich and Smith (1978)	Chalk	8	3.1
Kimura and Munakata (1992)	Crystalline	168	8
Kreft and others (1974)	Dolomite	22	44-110
Paschis and others (1989)	Basalt	9.1	1.7
	Basalt	9.1	1.8
	Basalt	33.5	1.6
	Basalt	14.6	4.0
	Basalt	12.8	.5
Rabinowitz and others (1977)	Limestone	32000	20-23
Tsang and others (1991)	Stripa	10-43	0.6-2.9
Webster and others (1970)	Schist and gneiss	538	134

Conceptual Model for Flow and Transport in Weathered Zone

The conceptual model for flow in the weathered zone is based on the characterization presented previously and information presented in Dutton and others (1994) and Mace (1994). The weathered zone is a thin skin ($\bar{x}_g$ = 8.6 ft [2.6 m]) on the outcrop of the Austin Chalk that exhibits local scale spatial continuity and that might be thinner in valleys and thicker on hillslopes and

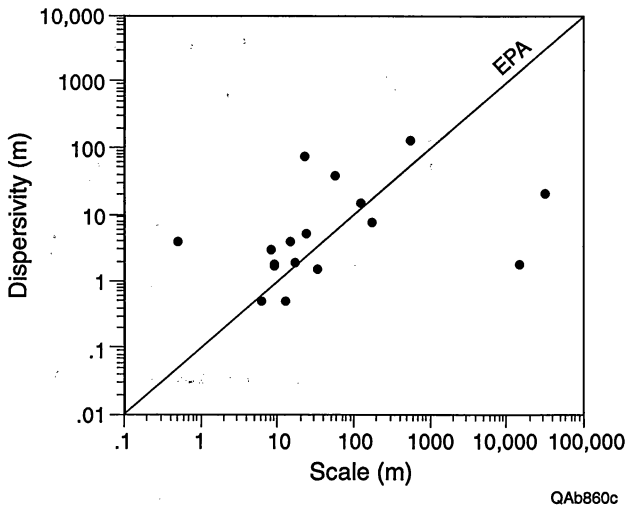

Figure 6. Relationship between dispersivity and scale in fractured rocks based on tracer tests. The line represents a mathematical relationship proposed by the EPA (1986) for transport problems.

hilltops. Where the Austin Chalk is faulted, weathering can have an effect at much greater depths, up to 80 ft (24 m), and flow through the weathered zone is locally focused toward and through the faulted zones. Transmissivity is variable in the weathered zone and decreases exponentially with depth. Presumably, fracture porosity also decreases with depth. The underlying, unweathered chalk has considerably lower permeability than the weathered zone, and therefore water flow is restricted in the unweathered bedrock.

Water levels in the weathered zone respond rapidly to rainfall and rise considerably. Because permeability is greater near the surface in the weathered zone, more water is presumably transported to local streams under a high water table than under a low water table. Solutes will also be rapidly transported, although there will be dilution by mixing with meteoric water. Ground-water gradients in the weathered and unweathered bedrock are topographically controlled, with a mean gradient of 0.01.

The weathered zone is susceptible to contamination due to its (1) proximity to the land surface and to potential contamination and (2) high permeability. Because the weathered zone discharges to local creeks and streams, surface water is also in danger of contamination. The soil zone probably offers little retardation because of preferential flowpaths (soil macropores, structure in smectite-rich soil) that direct water into the weathered chalk. Because fracture porosities are low and permeabilities are high, transport can proceed at a greater rate and affect large areas of shallow ground water.

Results of Modeling

Analytical Plume Solution

The analytical solution predicts the spatial distribution of solute through time and the arrival at observation points. The arrival time of half the maximum concentration ($C/C_o = 0.5$) at an observation point for a conservative and nondecaying solute directly down-gradient from the source is defined by the advective transport equation

$$t_{0.5} = \frac{n_f}{q} d = -\frac{n_f}{Ki} d \tag{5}$$

where $t_{0.5}$ is the time of arrival of half the maximum concentration, q is the darcy flux, n_f is the effective fracture porosity, K is the hydraulic conductivity, i is the hydraulic gradient, and d is the distance from the injection point to the observation.

Figure 7 shows the arrival times for $C/C_0 = 0.1$ and 0.5. The x axis has been generalized for mean water velocity, v_m, which includes hydraulic conductivity, hydraulic gradient, and effective porosity:

$$v_m = -\frac{Ki}{n_f} \tag{6}$$

The separation of the $C/C_0 = 0.1$ arrival time from the $C/C_0 = 0.5$ arrival time depends upon the dispersivity.

A "worst case" scenario would be based on the highest measured hydraulic conductivity that would result in the greatest solute velocity. For example, with a hydraulic conductivity of 64 ft d^{-1} (20 m d^{-1}), a fracture porosity of 0.2 percent (based on eq. 3), and a hydraulic gradient of 0.01, a contaminant would travel 1,000 ft (300 m) in about 3 days. However, the analytical solution does not consider recharge, the dynamic nature of water levels in the weathered zone, or the potential effects of diffusion into the matrix. The analytical solution should be considered a screening model: a simple approximation of the rate of transport in the weathered zone.

Cross-Sectional Model of Weathered Zone

The purpose of this model was to understand the ground-water dynamics in a weathered zone. It is assumed that all flow takes place in fractures and that the fracture network can be modeled as if it were equivalent to porous media. Figure 8 shows results from this model. The position of the water table in the weathered zone is dependent upon the amount of recharge where depth to water increases during periods of low recharge (fig. 8c).

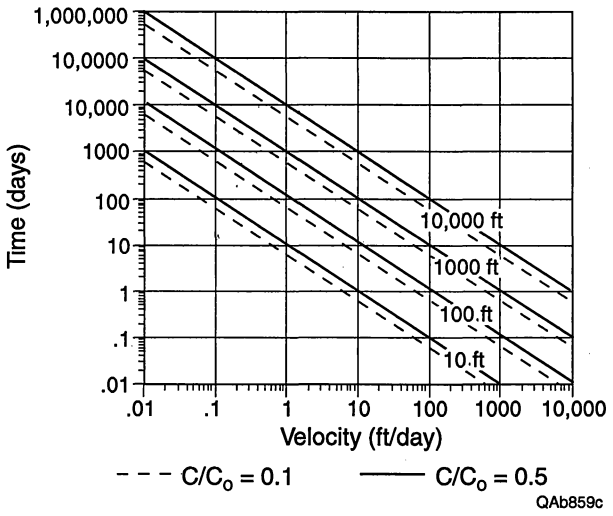

Figure 7. Breakthrough times for $C/C_0 = 0.1$ and 0.5 based on an analytical solution. The x axis has been generalized for mean water velocity.

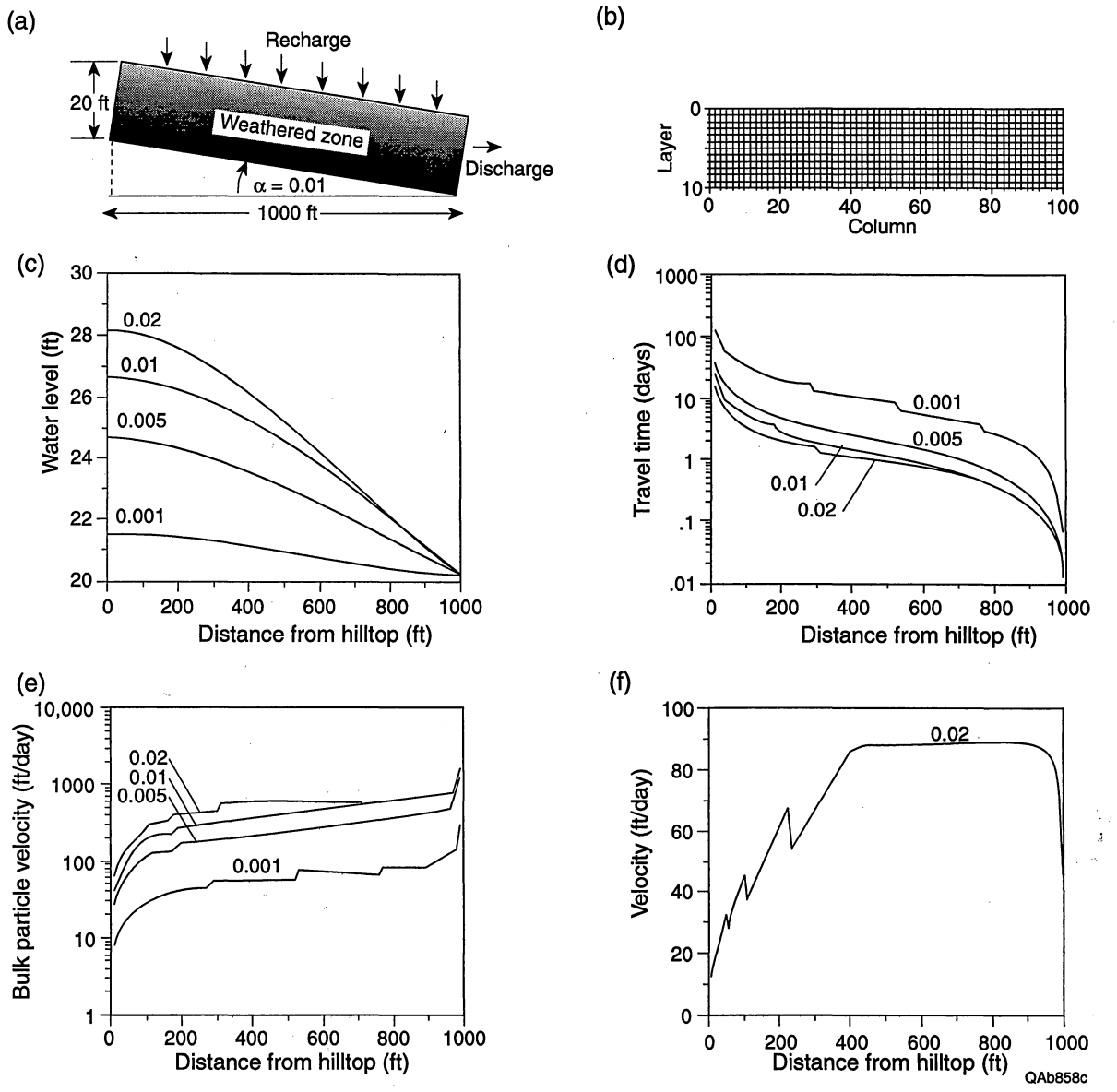

Figure 8. Ground-water flow and particle tracking using a cross-sectional, continuum, numerical model at recharge rates of 0.001, 0.005, 0.01, and 0.02 ft d^{-1}. (a) Conceptual model. (b) Model grid of 10 layers, 2 ft thick, and 100 columns, 10 ft wide. (c) Water levels. (d) Traveltimes of particles at different locations from the hilltop. (e) Bulk particle velocity determined by dividing the traveltime with the distance to the discharge point, or hill bottom. (f) Local particle velocity for a particle placed at the hilltop. Jaggedness of the plot is a consequence of model design and signifies the movement of the particle from a more conductive layer to a less conductive layer.

Figure 8d shows the time it takes a particle to move from the recharge point to the discharge point for different recharge rates (or water-table positions). The curves have an "S" shape with particles recharged near the hilltop having greater traveltimes than particles near the bottom. If each particle had the same transport velocity, the curves in figure 8d would be straight. Bulk particle velocity is the traveltime divided by the total lateral distance traveled (fig. 8e). Particles introduced at the top of the hill have a lower bulk particle velocity than particles introduced farther down the hill. This is due to vertical flow gradients at and near the top of the hill where flow is moving downward into less permeable intervals of the weathered zone. Particles introduced farther down the hill are introduced into more permeable intervals and tend to stay in these intervals because down-ward directed vertical gradients are not as strong. Figure 8f further demonstrates this effect by showing the velocity of a particle introduced at the top of the hill. Initially the particle moves downward in intervals with lower permeability, but it slowly moves upward through the weathered zone into more permeable intervals (the jaggedness in fig. 8f is due to the vertical discretization of the weathered zone). Finally, at the discharge point at the base of the hill, the particle moves upward owing to a small upward hydraulic gradient, which imparts a lower velocity.

As in the analytical solution, this model does not consider diffusion into the matrix, which may retard the movement of the solute. Diffusion effects on transport times are important at long water residence times. This effect can be assessed with an analytical solution that determines the arrival time, t_p, at a relative concentration of 0.5 of an injection of a nonsorbing solute into a stream of water flowing through porous fractured rock:

$$t_p = \left[\frac{\left(D_p\right)^{1/2} n_m a t_w}{0.954}\right]^2 + t_w \qquad (7)$$

where a is the wetted surface per volume of mobile water, t_w is the water residence time, D_p is the pore diffusivity, and n_m is the matrix porosity. For an completed wetted fracture surface, a is equal to the inverse of the fracture aperture. Figure 9 shows how D_p, n_m, and a can affect the arrival time of the solute front with parameter A defined as $D_p^{1/2} * n_m * a$. For the Austin Chalk, A is

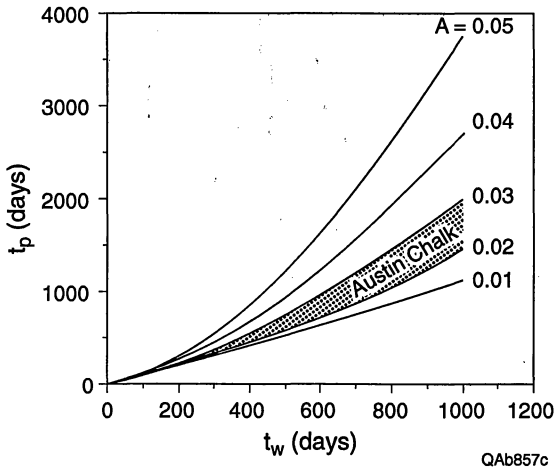

Figure 9. Influence of diffusion on transport through fractured rocks where t_p is the time for the peak concentration to arrive and t_w is the mean arrival time for the water. A is a function of pore diffusivity, matrix porosity, and the wetted surface per volume of mobile water.

estimated to be about 0.025 with D_p, n_m, and a equal to 10^{-9} ft^2 d^{-1} (10^{-10} m^2 d^{-1}), 0.25, and 3,000 ft^{-1} (10,000 m^{-1}), respectively. If the water residence time is 1,000 days, the solute arrival time (at $C/C_0 = 0.5$) would be about 1,500 days. For A equal to 0.025, solute transport is not strongly affected by diffusion for traveltimes less than 200 days. Therefore, traveltimes shown in figure 8d that are less than 200 days are unaffected by diffusion.

Transport modeling showed the effects of water-table position, vertical mixing, and recharge on transport in the weathered zone (fig. 10). Figure 10a shows that if solute transport was restricted to the uppermost portion of the weathered zone, solutes would arrive at 500 ft (150 m) down the hill in less than 2 days. If vertical mixing is allowed into underlying layers, solute arrival times are slowed 1 to 3 days. Recharge has the greatest effect on arrival times and maximum concentrations seen at the observation point with relative concentrations less than 0.2 after 5 days. Figure 10b and 10c shows the effects on the transport of a deeper water table. With the water table at the top of layer 5, or about halfway down the weathered zone, the arrival times of the solute are delayed 1 to 3 days. Arrival times are further delayed when the water table is at the top of layer 8, or three-quarters of the way down into the weathered zone.

Figure 11 shows solute concentration in the weathered zone at times 0.5, 1, 2, and 4 days for the cross-sectional model with constant head boundaries and the water table at the top of the weathered zone. At 0.5 days (fig. 11a) the solute is already transported halfway down the hill. At 4 days (fig. 11d), high concentrations exist in almost the entire model domain. Figure 12 shows the distribution of solutes in the weathered zone at times of 0.5, 1, 2, and 4 days for the model with recharge. The permeability distribution between the model shown in figures 11 and 12 is the same. The main difference between the two models is the influence of recharge and hydraulic gradients. Because the model used in figure 11 had constant head boundaries at each end of the model, the hydraulic gradient directed from one end of the model toward the other is constant. Hydraulic gradients for the recharge model (fig. 12) are much lower at the hilltop (for example, see fig. 8c) and have a downward component.

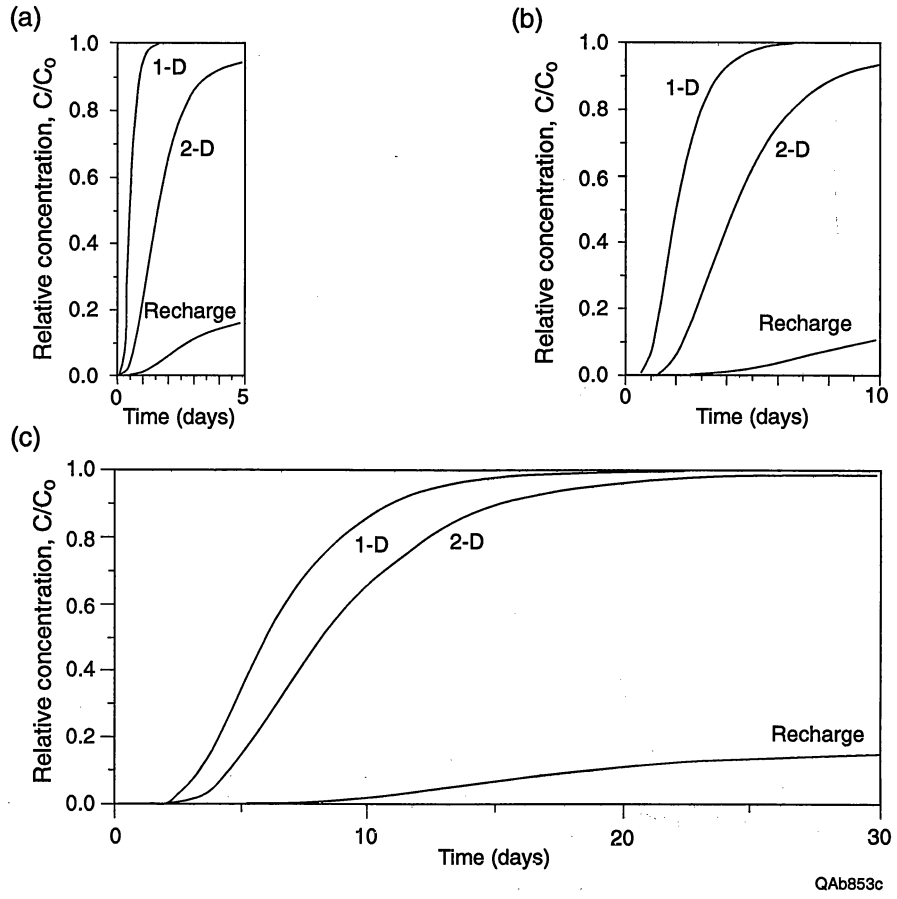

Figure 10. Breakthrough curves for solute transport through the (a) entire depth (layers 1–10), (b) lower half (layers 5–10), and (c) lower quarter (layers 8–10) of the weathered zone. Each plot includes results from three simulations: (1) one-dimensional transport only through the highest active layer (layer 1 for [a], layer 5 for [b], and layer 8 for [c]), (2) two-dimensional transport through all the active layers, and (3) two-dimensional transport with recharge. The 1-D and 2-D models had constant heads along each end to result in a gradient of 0.01. The recharge model only had a constant head (set at land surface elevation) on the downgradient side, and recharge rate was adjusted until water levels reached the top of the highest active layer ($R = 0.02$ ft d^{-1} for [a], 0.0019 ft d^{-1} for [b], and 0.00032 ft d^{-1} for [c]). The source was placed in cells 2 through 4, at land surface, in the highest active layer.

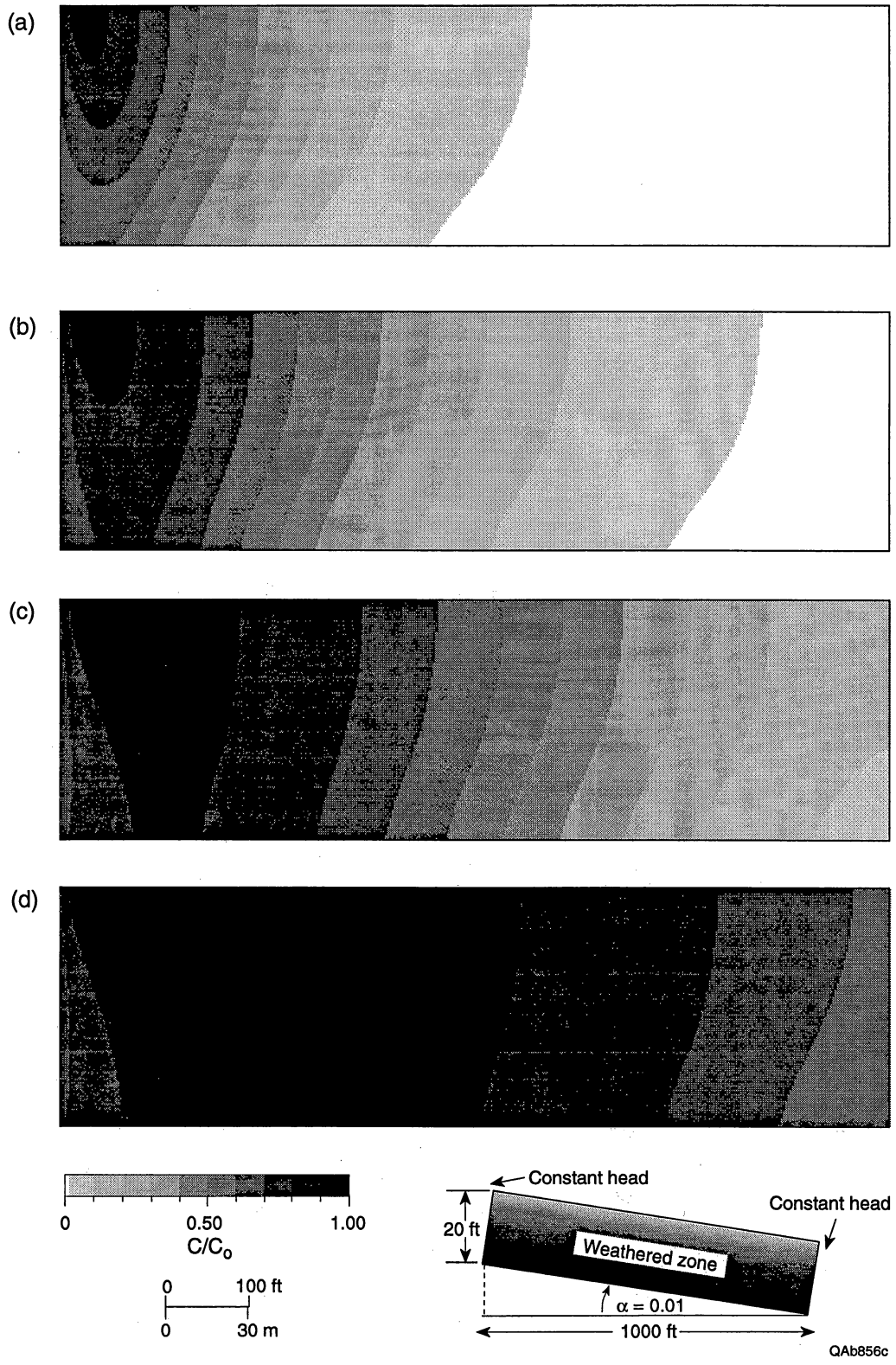

Figure 11. Concentration profiles after (a) 0.5, (b) 1, (c) 2, and (d) 4 days for the cross-sectional model with constant head boundaries at ends. Conceptual model shown in lower right.

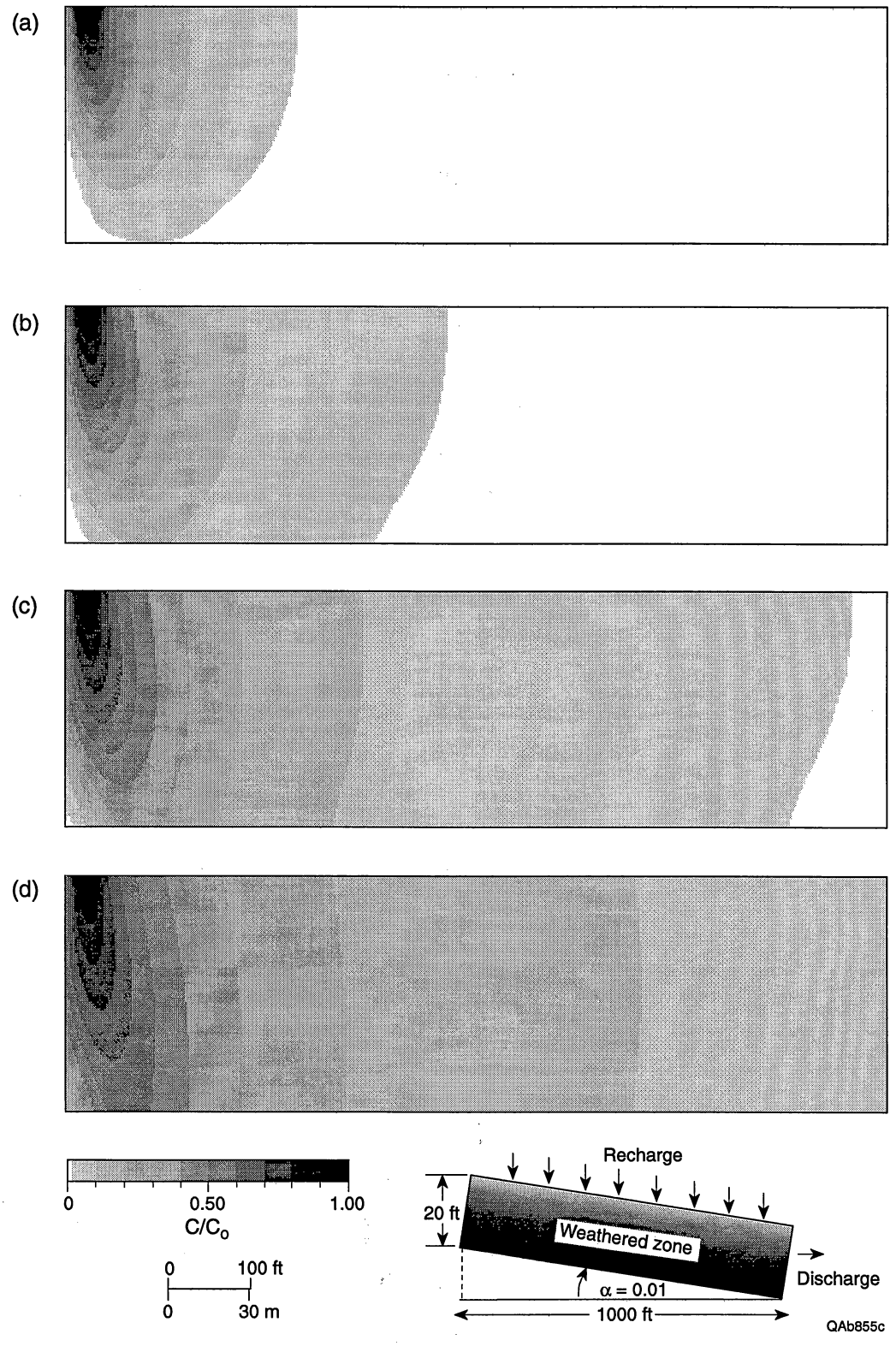

Figure 12. Concentration profiles after (a) 0.5, (b) 1, (c) 2, and (d) 4 days for the cross-sectional model with recharge. Conceptual model shown in lower right.

Model of Ground-Water Flow and Transport on the West Campus

The potentiometric surface predicted by the numerical model for recharge rates of 0.01 and 0.001 in d^{-1} (0.003 and 0.0003 m d^{-1}) (fig. 13) approximates water levels mapped in the West Campus area from hand-dug wells (Mace and Dutton, 1994a). Differences between the two recharge scenarios are subtle: equipotential lines for a recharge rate of 0.01 in d^{-1} (0.003 m d^{-1}) are displaced upgradient a small distance. This same effect has been found in water-level maps of the West Campus weathered zone.

Figure 14 shows results from tracking particles through the model. These plots represent traveltimes and mean path velocities for the model with recharge at 0.01 ft d^{-1} (0.003 m yr^{-1}) determined by placing particles in each active cell of the fifth layer and tracking them to their discharge points. Figure 14a shows the distribution of the log of the traveltime, which has a geometric mean of 16 days. Therefore, most of the particles require 16 days to move from their initial position to their discharge point. The range in time is from over 10,000 days to under 1 day. Figure 14b shows the velocity of the particles with a geometric mean of 158 ft d^{-1} (48.2 m d^{-1}). This suggests, in conjunction with the traveltime, that the most common travel distance is 2,530 ft (770 m).

Limitations of the Numerical Modeling

The numerical modeling is limited owing to (1) inadequacies in the characterization of the weathered zone, (2) the assumptions inherent in the conceptual models used for modeling, and (3) the numerical approach. The cross-sectional models used in this report assume constant weathered zone thickness and hillslope. In reality, the weathered zone varies in thickness, and the topography is not uniformly linear. Additional complexity can be added to these models by considering these variations. The numerical model assumed that the fractures could be treated as porous media. This may be true for fractures near the land surface where fracture density is high, but may not be as applicable at depth where there are fewer fractures. This complicates transport

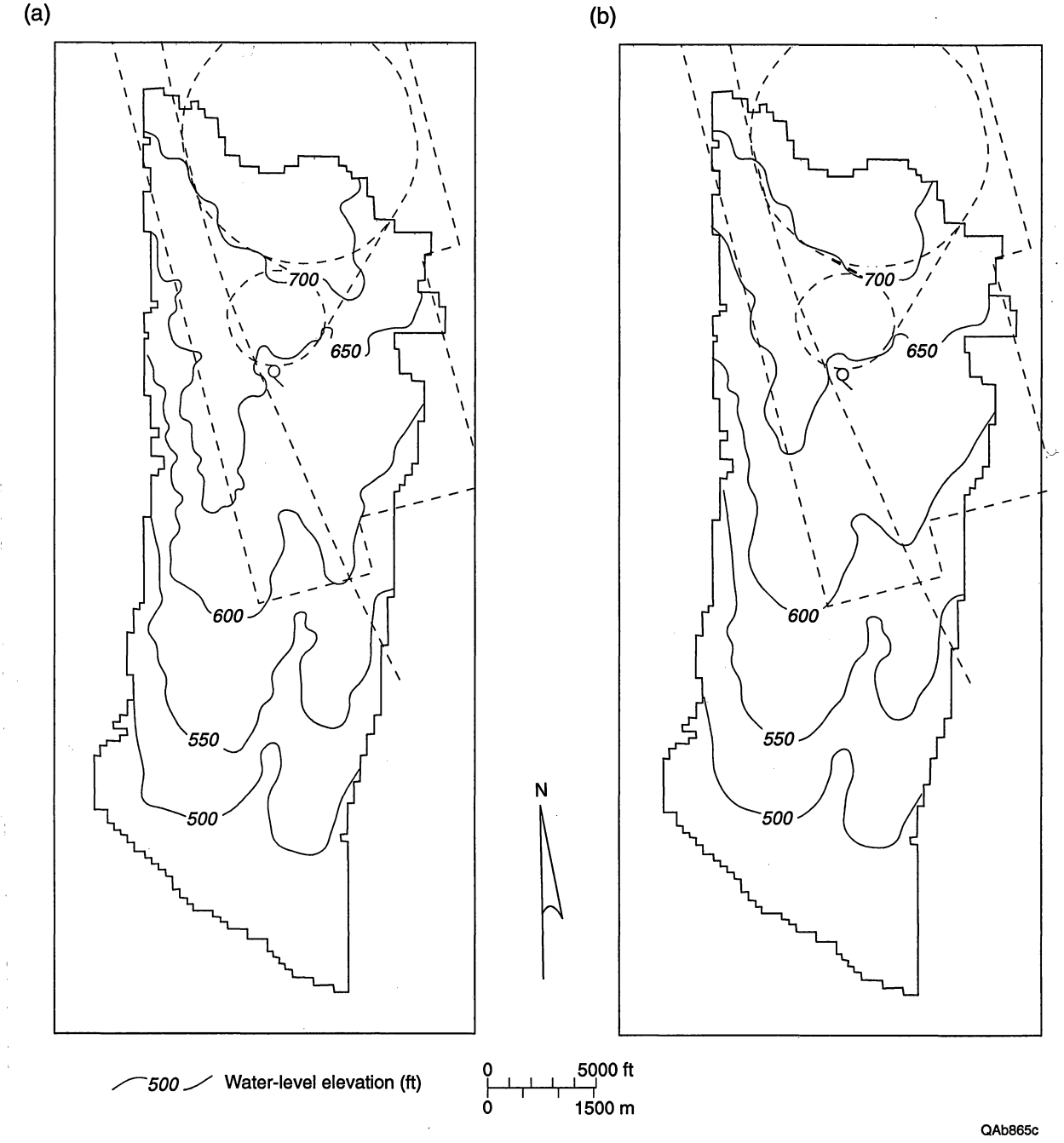

Figure 13. Potentiometric surfaces predicted with the numerical model for recharge rates of (a) 0.01 ft d^{-1} and (b) 0.001 ft d^{-1}.

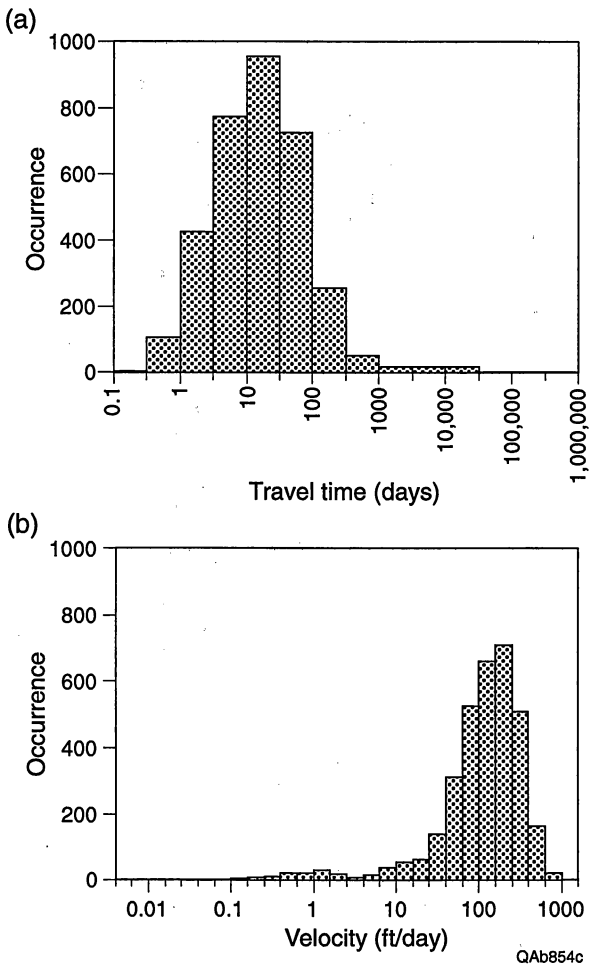

Figure 14. Results of (a) traveltime and (b) mean velocities of particle tracking with the West Campus weathered-zone model.

simulations because a single fracture or group of interconnected fractures could transmit solutes at a much faster rate than predicted with a continuum approach. It is unclear how hydraulic properties vary over short distances at the SSC site. Because the weathered zone is fractured, one might expect permeability to vary considerably. In this case, the assumption of a constant lateral hydraulic conductivity is suspect. Lateral variations in hydraulic conductivity might serve to speed or slow down the movement of solutes.

Transport parameters such as longitudinal, transverse, and vertical dispersivity are estimates and therefore are highly uncertain. Furthermore, by using a continuum model, it is assumed that Fickian dispersion applies, which might not necessarily be true in fractures, especially over short distances. In addition, the model assumes that solutes are nonsorbing and nondecaying.

CONCLUSIONS

The weathered zone of the Austin Chalk is a complex, fractured hydrologic system with the potential to rapidly transport solutes. Hydraulic conductivity and fracture porosity decrease with depth in the weathered zone, with hydraulic conductivity possibly decreasing exponentially and porosity decreasing as the cube root of the hydraulic conductivity of the fractured interval. Because the weathered zone is thin relative to local changes in topography, the direction and magnitude of topographic slope are good indicators of the direction and magnitude of hydraulic gradient, and therefore ground-water flow, in the weathered zone. Mean slope is scale dependent and is about 0.01 for a length of 3,000 ft (1,000 m).

Numerical modeling shows that ground-water travel times depend on vertical variations in hydraulic conductivity, water-table position, and point of entry into the flow system. Recharge controls the water-table position, which in turn controls the thickness of permeable intervals that are saturated with water. Traveltimes at lower water-table positions (low recharge) can be ten times longer than traveltimes in higher water-table positions (high recharge). Water that enters near the top of a hill has a longer residence time because of the greater distance to the discharge point (creek bottom, seep, or spring) and lower hydraulic gradients near hilltops. Geometric mean residence

time for water in the weathered zone under wet conditions at the SSC site is about 16 days with a geometric mean velocity of 158 ft d^{-1} (48.2 m d^{-1}).

Water-table position, vertical mixing, and recharge affect solute transport in the weathered zone. Lower water tables intersect less-permeable intervals in the weathered zone and therefore increase the traveltime of solutes. Vertical mixing within the weathered zone slows solute arrival times 1 to 2 days. Recharge also considerably slows solute arrivals and greatly reduces the maximum observed concentrations.

ACKNOWLEDGMENTS

This research was performed for and funded by the Texas National Research Laboratory Commission (TNRLC) under contract no. IAC 94-0108. I thank Alan Dutton, Eddie Collins, Bill Mullican, Dave Goss, Bridget Scanlon, Jack Sharp, Ian Jones, and Jim Mayer for helpful comments and discussion concerning this work. Steven Rooks, Gordon "Cookie" Forman, and William Doneghy helped greatly with field work and testing. Susan Lloyd did the word processing and pasteup. Nancy Cottington drafted the figures under the direction of Richard L. Dillon. Jeannette Miether edited the paper.

REFERENCES

Bear, Jacob, 1972, Dynamics of fluids in porous media: Elsevier, New York, 764 p.

Bentley, H. W., and Walter, G. R., 1983, Two-well recirculating tracer test at H-2: Waste Isolation Pilot Plant (WIPP), Southeast New Mexico: Draft, Hydro Geochem., Inc., Tucson AZ.

Classen, H. C., and Cordes, E. H., 1975, Two-well recirculating tracer test in fractured carbonate rock, Nevada: Hydr. Sciences, Bulletin des Sciences Hydrologiques, v. 20, no. 3, p. 367–382.

Collins, E. W., Hovorka, S. D., and Laubach, S. E., 1992, Fracture systems of the Austin Chalk, North-Central Texas, *in* Schmoker, J. W., Coalson, E. B., and Brown, C. A., eds., Geological Studies Relevant to Horizontal Drilling: Examples from Western North America: Rocky Mountain Association of Geologists, p. 75–88.

Dieulin, A., 1981, Lixiviation in situ d'un gisement d'Uranium en Millieu Granitique: Draft report No. LHM/RD/81/63, Ecole Nationale Superieure des Mines de Paris, Fontainebleu, Cedex, France.

Dutton, A. R., Collins, E., Hovorka, S., Mace, R. E., Scanlon, B., and Xiang, J., 1994, Occurrence and movement of ground water in Austin Chalk, Eagle Ford, and Ozan Formations at the Superconducting Super Collider (SSC) site, Ellis County, Texas: The University of Texas at Austin, Bureau of Economic Geology, topical report prepared for Texas National Research Laboratory Commission under contract no. IAC(92-93)-0301, 393 p.

Earth Technology Corporation, 1990, Hydrogeologic conditions at the Superconducting Super Collider Site: Long Beach, California, Project No. 87-888-0017, Report No. SSC-GR-63, variously paginated.

EPA, 1986, Federal Register: v. 51, no. 9, p. 1652.

Gelhar, L. W., Mantoglou, A., Welty, C., and Rehfeldt, K. R., 1985, A review of field-scale physical solute transport processes in saturated and unsaturated porous media: Electric Power Research Institute EPRI-4190 Project 2485-5, 166 p.

Goblet, P., 1982, Interpretation d'experiences de tracage en Milieu Granititque (Site B): Report LHM/RD/82/11: Fontainebleu, Cedex, France, Centre d'Information Geologique, Ecole Nationale Superieure des Mines de Paris.

Grove, D. B., and Beetem, W. A., 1971, Porosity and dispersion constant calculations for a fractured carbonate aquifer using the two-well tracer method: Water Resources Research, v. 17, no. 1, p. 128–134.

Haldeman, W. R., Chuang, Y., Rasmussen, T. C., Evans, D. D., 1991, Laboratory analysis of fluid flow and solute transport through a fracture imbedded in porous tuff: Water Resources Research, v. 27, no. 1, p. 53–66.

Hunt, B., 1978, Dispersive sources in uniform ground-water flow: Journal of Hydraulics Division, ASCE, v. 104, no. HY1, p. 75–85.

Ivanovich, M., and Smith, D. B., 1978, Determination of aquifer parameters by a two-well pulsed method using radioactive tracers: Journal of Hydrology, v. 36, p. 35–45.

Kimura, Hideo, and Munakata, Masahiro, 1992, Validation studies of tracer tests in a fracture zone at the Finnsjon research area: Advances in Water Resources, v. 15, p. 63–74.

Kreft, A., Lenda, A., Turek, B., Zuber, A., Czauderna, K., 1974, Determination of effective porosities by the two-well pulse method: Isotope Techniques in Ground Water Hydrology: Vienna, IAEA, v. 2, p. 295–312.

Mace, R. E., 1993, Modeling of ground-water flow in subsurface Austin Chalk and Taylor Marl in Ellis County, Texas, near the superconducting super collider site (abs.): Geological Society of America, South-Central Section, Abstracts with Programs, v. 25, no. 1, p. 37.

Mace, R. E., 1994, Hydrologic studies in fractured chalk in the vicinity of the SSC site: Data report for the TNRLC under contract no. IAC(92-93)-0301, 41 p.

Mace, R. E., and Dutton, A. R., 1994a, Record of Water levels measured in SSCL monitor wells and private wells at the SSC site, Ellis County, Texas: Data report for the TNRLC, 236 p.

Mace, R. E., and Dutton, A. R., 1994b, Hydrogeologic controls on contaminant transport in weathered and fractured chalk, *in* Dutton, A. R., ed., Toxic substances and the hydrologic sciences: American Institute of Hydrology, p. 535–546.

Marrett, Randall, submitted, Permeability, porosity, and seismic anisotropy from scaling of open fracture populations: Department of Geological Sciences, The University of Texas at Austin, submitted to Geology.

McDonald, M. G., and Harbaugh, A. W., 1988, A modular three-dimensional finite-difference ground-water flow model: U.S. Geological Survey Techniques of Water-Resources Investigations, book 6, variously paginated.

Nelson, R. A., 1987, Fractured reservoirs, turning knowledge into practice: Houston, Gulf Publishing, 320 p.

Paschis, J. A., Koenig, R. A., Benedik, J. E., Jr., and Steele, T. D., 1989, Application of data-logger/pressure-transmitter/conductivity-probe instrumentation in long-term salt-tracer studies in a fractured, saturated geologic medium: New field techniques for quantifying the physical and chemical properties of heterogeneous aquifers: Dallas, Texas, Proceedings of the National Water Well Association Meeting, p. 317–338.

Pollock, D. W., 1989, Documentation of computer programs to commute and display pathlines using results from the U.S. Geological Survey modular three-dimensional finite-difference ground-water flow model: Washington, D.C., Scientific Software Group, variously paginated.

Rabinowitz, D. D., Gross, G. W., and Holmes, C. R., 1977, Environmental tritium as a hydrometeorologic tool in the Roswell Basin, New Mexico, I. Tritium input function and precipitation-recharge relation: Journal of Hydrology, v. 32, p. 3–17.

Snow, D. T., 1969, Anisotropic permeability of fractured media: Water Resources Research, v. 5, p. 1273–1289.

Tsang, C. F., Tsang, Y. W., and Hale, F. V., 1991, Tracer transport in fractures: analysis of field data based on a variable-aperture channel model: Water Resources Research, v. 27, p. 3095–3106.

Webster, D. S., Proctor, J. F., Marine, J. W., 1970, Two-well tracer test in fractured crystalline rock: USGS Water Supply Paper No. 1544-I.

Wilson, J. L., and Miller, P. J., 1978, Two-dimensional plume in uniform ground-water flow: Journal of Hydraulics Division, ASCE, v. 104, no. HY4, p. 503–514.

Zheng, C., 1992, A modular three-dimensional transport model for simulation of advection, dispersion, and chemical reactions of contaminants in groundwater systems (MT3D version 1.5): Bethesda, Maryland, S.S. Papadopulos and Associates, Incorporated, variously paginated.

Appendix A. Determination of fracture porosity from continuum scale hydraulic conductivity measurements.

A relationship based on the mathematical definitions of porous media and fracture permeability was derived to estimate fracture porosity from measures of continuum scale hydraulic conductivity. Hydraulic conductivity, K, is defined as

$$K = \frac{\rho g}{\mu} k \qquad \text{(A1)}$$

where ρ is the density of water, g is the acceleration due to gravity, μ is the dynamic viscosity, and k is the intrinsic permeability. For porous media, k is a function of the geometric properties of the media. The intrinsic permeability of a fracture, k_f, is defined as

$$k_f = \frac{e^2}{12} \qquad \text{(A2)}$$

where e is the fracture aperture (Snow, 1968).

Hydraulic conductivity measurements of the weathered zone have been interpreted assuming that the fracture network can be modeled as if it were equivalent to porous media. Therefore, a relationship between porous media permeability and fracture permeability needs to be derived. This is done by using Darcy's law

$$Q = -KAi \qquad \text{(A3)}$$

where Q is the volumetric flux, A is the cross-sectional area perpendicular to flow, and i is the hydraulic gradient and setting the volumetric flux of a porous media, Q_m, equal to the volumetric flux of a fracture, Q_f:

$$Q_m = Q_f \qquad \text{(A4)}$$

Substituting A3 into A4a:

$$-K_m A_m i = -K_f A_f i \qquad \text{(A5)}$$

Let A_m be L^2 where L is a unit length of a block of porous media and A_f be e^*L where L is the same length as before, but represents a fracture length. After substituting eq. A1, A_m and A_f into A5, canceling out -1, i, ρ, g, μ, and L, and solving for e, the following is attained:

$$e = (12k_m L)^{1/3} \tag{A6}$$

Fracture porosity, n_f, for area L^2 is defined as e/L. Therefore, by dividing A6 by L, fracture porosity is determined from porous media permeability with:

$$n_f = \frac{e}{L} = \frac{(12k_m L)^{1/3}}{L} \tag{A7}$$

This relationship is based on using an equivalent, single fracture to represent the porous media permeability. A general relationship for more than one fracture is

$$n_f = \frac{N\bar{e}}{L} = \left(\frac{12k_m L}{N}\right)^{1/3} \frac{N}{L} \tag{A8}$$

where $\bar{e}$ is the mean fracture aperture and N is the number of fractures per length L (or, total length of the fractures divided by L). For multiple fracture systems, porosity increases by $N/N^{1/3}$ for increasing numbers of fractures. Therefore, equation A7 will underestimate fracture porosity if there is more than one fracture. However, fracture apertures often follow fractal, or power-law, distributions, in which case the fractures with the larger apertures control the permeability and flow, whereas the other fractures account for most of the fracture system porosity (Nelson, 1987; Marrett, submitted). In this case, equation A7 may be the best method to estimate effective fracture aperture involved in transport.

Appendix B. Soil and weathered-zone thicknesses measured in SSC boreholes.

Well number	Soil thickness (ft)	Weathered thickness (ft)	Topographic setting	Notes
B-6		4.5	-	
B-C1		3	M-L	
B-RR		6.5	-	
B1.1	0.5	6.7	M-L	
B1296	0.5	14	H-M	
B12A	4.7	3.1	L	
B13	5	7.2	L-M	
B1316	2	10.5	H	
B14	2	12.9	L	
B15	1	9	M-L	
B1527	20	10.4	L-M	
B1533	0.5	15.8	L-M	
B16	0.5	20.9	M	
B1737	4.5	10	H	
B1807	1.5	12	H	
B20-89	0.5	9.5	H-M	
B20-89	0.5	9.5	H-M	
B2052	4	5.5	H	
B2062	3.5	17.5	H	
B22-99	0.5	6.6	H	
BE1	1	14.6	M	
BE1	4.2	6.8	M	
BE1-90	2	11.4	H	
BE1.6	0	2.9	M	
BE1.7	18	9.85	H	
BE10	2.5	2.3	L	
BE10.5	14.5	3.3	H	
BE10.7	1	3.5	H-M	
BE10.9	6.5	13.5	M-L	1
BE10.9A	4	4	M-L	
BE2		9.2	H	
BE3	1	80.2	M	2
BE4	30	13.3	M	
BE9	37.5	4.3	M	
BF10.1	2.5	12.4	M	
BF2	0.5	7.5	M	
BF3		2.1	H	
BF9	16	12.75	M-H	
BIR11	1	2	M	
BIR12	2.5	7.2	M	
BIR13	2	5	M	
BIR14	1.7	4.3	M	
BIR21	1	3	H	
BIR22	0.5	17.7	H	
BIR23	2	12.4	H	

Well number	Soil thickness (ft)	Weathered thickness (ft)	Topographic setting	Notes
BIR31	2.4	15.1	H	
BIR32	6	13.2	H	
BIR33	1.5	11	H	
BIR41	4	12	H	
BIR42	1.5	10.6	H	
BIR43	0.5	4.8	H	
BIR44	2	5.8	H	
BIR45	1	12.8	H	
BIS40		12.3	-	
BK1	3	2.3	M	
E-4		4.8	-	
F-2		11.3	H	
F-3		1	-	
J-2		16	H	
J-3		9	L	
J-6		3	H	
K-1		6.1	H	
K-2		12.4	H	
MB-1	0.3	24.5	M	
MB-2	7.9	16.5	M	
MB-3	21.7	1.3	M	
MB-4	5.2	10.4	M	
MB-5	13.2	8	M	
MB-6	0.5	6.4	M	
MB-7	0.8	9.45	M	
MB-8	3.2	11.35	M	
MB-9	13.1	16.9	M	
MB19	2.3	10.9	M	
MB20	2.7	14.05	M	
MB21	0.6	24.95	M	
MB22	0.5	22.8	M	
MB23	0.9	25.6	M	
MB24	0.5	69.2	M	
MEB 7	4.5	6.3	M	
MEB 8	1.5	17.9	M	
MEB-10	3	10.85	H	
MEB-11	1.5	11.85	H	
MEB-12	2.5	24.4	M	
MEB-13	1	21.5	M	
MEB-14M	3	6	M	
MEB-15M	2.5	24.1	M	
MEB-16	3.5	65.6	M	
MEB-17S	3.5	6.7	M	
MEB-18S	3.5	11.7	M	
MEB-19S	3	12.5	M	
MEB-1P	7.5	3.8	M	
MEB-2	3.5	10.75	M	
MEB-20S	5	65.5	H-M	
MEB-21S	2.5	7.5	H	

Well number	Soil thickness (ft)	Weathered thickness (ft)	Topographic setting	Notes
MEB-22S	0.5	25.5	H-M	
MEB-23S	5.25	7.75	M	
MEB-24S	5.5	11.95	M	
MEB-25S	3	2.5	M	
MEB-26S	8	9.4	M	
MEB-27	2.5	11.65	M	
MEB-28	12	5.7	M	
MEB-29	9	10.45	M	
MEB-3	13.8	6.2	M	
MEB-30	5	10.5	M	
MEB-31	1.5	16.05	M	
MEB-32S	1.5	21.3	M	
MEB-33	5	5	M	
MEB-34	3	32	M	
MEB-35	0.5	14.5	M	
MEB-36	3.5	6	M	
MEB-4	13	4.65	M	
MEB-5	13.5	4.5	M	
MEB-9	4	4.5	M	
MEB6P	7.5	9.5	M	
SE1	0.5	24.7	M-L	
SE1.2A	8	3	M	
SE1.2A	8	3	L	
SE1.2B	32	3	M	
SE1.2B	32	3	L	
SE1.5A	1	22	M-L	
SE1.5B	2.5	16.5	M-L	
SE1.5B	2.5	16.5	H-M	
SE1.8	1	28.8	M	2
SE10.4	0.5	12	H	
SE10.8	0.5	7.5	L	
SE10.9C	3.5	8.85	M	
SE10.9D	3.5	7.6	M	
SE4.6	13.8	19.2	H	
SE4.7	13.1	14.5	H	
SF10.1	3	16	M	
SF10.1A	1	10	M-L	
SF10.1B	8.5	10.5	M-L	
SF10.1C	0	57.7	M-L	3
SF10.6A	1	8.5	H	
SF10.6B	6	15	H	
SF8.3A	22	8.2	M	
SF8.3B	15	16	M	
SF8.3C	20.5	7.5	M	
SF8.3E	17.9	8.6	M	
SF8.3F	16.5	8.5	M	
SI2A	1	13	M	
SI2B	3.5	19.5	M	

Well number	Soil thickness (ft)	Weathered thickness (ft)	Topographic setting	Notes
SI2C	14.4	1.45	M	
SIR3A	3	14	H-M	
SIR3B	3	10.6	H-M	
T-1		10.4	-	
T-3		5.9	-	
VE3.5	7.5	2.5	M	
VE3.5A	3	2	H-M	
VE9.3	20	8	M	
VRI1.7	21	1.5	L	

- Undetermined
[1] Also weathered from 68 to 88 ft
[2] Possibly in a faulted zone
[3] In a fault zone